Characterization of x-shaped nanoaperture antenna arrays operating in mid-infrared regime

Mustafa Turkmen[1,2,3]

[1]*Department of Electrical and Computer Engineering and* [2]*Photonic Center, Boston University, Boston, MA, 02215, USA*

[3]*Department of Electrical and Electronics Engineering, Erciyes University, 38039, Kayseri, Turkey*

Corresponding author: turkmen@bu.edu

Received February 28, 2013; accepted April 19, 2013; posted online June 21, 2013

The characterization of x-shaped antenna arrays operating in the mid-infrared is proposed. An equivalent circuit model for the resonant characteristic of the x-shaped nanoaperture antenna arrays is also included. In order to understand the resonance behavior of the structure, a detailed study of the field-enhancement capabilities and light transmission characteristics of the structure is proposed. In the experimental studies, the transmission characteristics of the periodic x-apertures are analyzed by varying the geometrical dimensions. Consequently, it is observed that the periodic subwavelength x-apertures show extremely high near-field optical resolution and enhanced transmission compared with the other nm-sized apertures.

OCIS codes: 050.6624, 230.5750, 130.3060, 160.4760

doi: 10.3788/COL201311.070501.

Nanoscale subwavelength apertures are the key elements for near-field optical engineering applications. Therefore, many theoretical and experimental studies have been carried out to explain the underlying physical phenomena of near-field enhancement with a metal film which is perforated with a periodic subwavelength aperture array[1-25]. Metallic nanostructures with sharp corners and edges that form a pointed tip provide a convenient way for extremely high light confinement with long cutoff wavelength due to its advantage of blocking the background light thanks to their sharp edges. However, circular or square apertures with dimensions that are much smaller than the wavelength of light suffer from very low transmission. Changing the aperture shape, diameter, refractive index of the adjacent medium, and film thickness of the structures has been shown to significantly improve their optical transmission[4-16]. They provide enhanced near-field transmission with tunable resonances from infrared (IR) to visible wavelengths, which are very important for chip-based optical devices, active filters, and bio-sensors[17-20]. Consequently, many periodic subwavelength aperture designs, such as cross-, H-, and C-shaped structures, bowties, dimmers, elliptics, and fractals, have been performed for obtaining high field confinement and enhancement[1-25]. Bowtie-shaped nanoantennas have been used to provide focused spots for many applications, including nanoscale lithography fabrication[21], data storage[22], and single-molecule fluorescence measurement[23]. As another ridge-shaped geometry x-shaped apertures have been studied for different purposes[16,24,25]. For instance, they have been patterned onto the Au coated facet of a quantum cascade laser application in Ref. [24], and fabricated on a Ag film sputtered glass slide using focused-ion-beam (FIB) technique in Ref. [25]. However the main difference of the x-shape among the other aperture geometries is its angle, and no angle change has been studied before. Moreover, in this letter we focus on the structures operating in the mid-IR regime.

We experimentally measured and theoretically analyzed the light transmission characteristics of x-shaped subwavelength apertures for operating in the mid-IR. An equivalent circuit model for the x-shaped nanoaperture antenna arrays is also proposed. Before equivalent circuit modelling, periodic subwavelength x-apertures are analyzed through finite difference time domain (FDTD) simulations. It is observed that x-apertures with an exclusive design composed of four metallic tips facing each other (Fig. 1) enable nanoscale light concentration and enhanced optical transmission via propagating waveguide mode within the gap. Moreover, a lift-off free e-beam lithography (EBL) approach is presented for on-chip fabrication of x-aperture antenna arrays. The periodic nanoscale x-aperture arrays are fabricated on a thin Au film, which is perforated on a free standing membrane. The spectral dependence on the geometrical parameters for controlling the resonance frequencies is determined using Fourier transform infrared (FTIR) spectroscopy. Due to the tunability of the spectral response and enhanced near-field confinement capabilities, x-aperture arrays operating in the mid-IR can be used for a wide range of applications such as active filters and bio- and chemical-sensing.

Figure 1 shows the schematic view of the x-shaped nanoaperture antenna design and a SEM image of the structure. In Fig. 1(a), the geometrical parameters are, L, length of the aperture, w, aperture width, and θ, angle. For the numerical analysis, the structure is modeled by three-dimensional (3D)-FDTD method[26]. In the numerical setup, along x and y axes periodic boundary conditions are used, whereas perfectly matched layer is used along $\pm z$ axis, which also corresponds to the direction of the illumination light source. Herein, to obtain high optical transparency, the structure under study stands on a SiN_x substrate with refractive index of 2.16. The frequency dependent dielectric constants of Ti and Au are taken from Ref. [27]. In the simulations, the thicknesses of Au, and Ti layers are chosen as $t_{\mathrm{Au}} = 30$ nm and $t_{\mathrm{Ti}} = 5$ nm, respectively. Figure 2 shows the spectral response and total electric field intensities, $|\mathbf{E}|^2$, at the air-metal interface (top surface of the x-apertures) for the corresponding resonance peak. To determine a

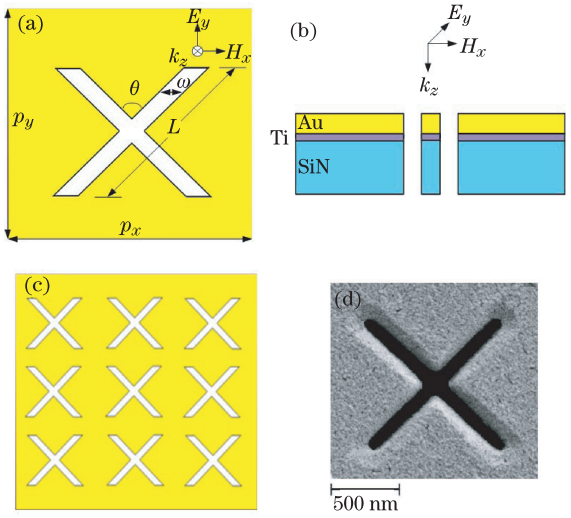

Fig. 1. (a) Schematic view of x-apertures, (b) cross-section view, (c) top view, and (d) SEM image of the fabricated structure with corresponding parameters: $p_x = p_y = 2000$ nm, $L = 1200$ nm, $\omega = 100$ nm, and $\theta = 90°$.

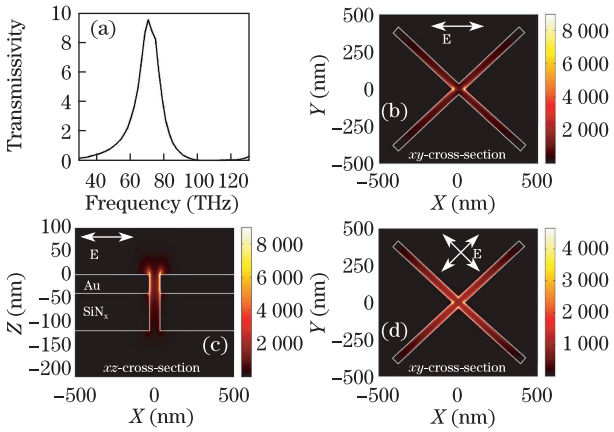

Fig. 2. (a) Transmission spectra of a subwavelength x-aperture array, and total electric field intensities at the corresponding resonance peak for an x-polarized light source (b) xy- and (c) xz-cross-section views, and (d) xy-cross-section for an unpolarized light source ($p_x = p_y = 2\,000$ nm, $L = 1200$ nm, $\omega = 50$ nm, and $\theta = 90°$).

resonance around 70 THz as shown in Fig. 2(a), one can only change the dimensions of the structure, such as L, or ω. The transmissivity (number of transmitted photons / number of expected transmitted photons from the conventional transmission theory) spectra of the periodic x-apertures with the same open area are shown in Fig. 2(a). In Figs. 2(b) and (c), the total electric field intensities of the x-shaped nanoaperture arrays are given in xy and xz cross-sections. Figure 2(d) demonstrates the near-field enhancement capacity of the proposed nanoantennas under an unpolarized illumination source. For the x-shaped aperture, the transmitted field has 8000 times more intensity than the illumination field while that for the rectangular aperture is around 160 times. This provides the near-field resolution capability of the x-shaped structures over the conventional ones. This is highly desirable for bio- and chemical-sensing applications as it increases the overlap between the electromagnetic fields of the surface plasmons and the analytes or molecules in the surrounding medium.

For the subwavelength structures, it is highly desirable to characterize the structures and to understand the physical origin of the spectral dependence in determining control mechanisms of the resonant behavior of the structure[13-15]. Therefore, in the experimental studies, we characterize the x-shaped nanoapertures by varying geometrical parameters. Our fabrication process consists of three steps: fabrication of the free standing membrane, patterning the apertures to the membrane, and deposition of metallic layers[14,15]. In the first step, we fabricated free standing membranes using a multilayered SiNx wafer, which consisted 550-μm silicon wafer coated with 400-nm-thick SiNx on each side. For the nanoaperture patterning to the positive e-beam resist, poly (methylmethacrylate) (PMMA) was coated to the membrane. PMMA spinning was then performed followed by e-beam exposure using Zeiss Supra 40VP. After the development of PMMA, patterns were transferred to the SiNx membrane by dry etching with the use of SF_6 and Ar gases. The EBL written patterns were removed by Methlisobutyl-ketone (MIBK)-IPA solution and x-aperture arrays were fabricated on the free standing membranes by RIE etching. Finally, directional Au deposition was performed in CHA-600S e-beam evaporator for 30-nm-thick Au film after depositing 5-nm-thick prior adhesion Ti layer. Transmission spectra were recorded using a Bruker^{TM} FTIR.

Figure 3 shows the changes in the spectral response for different length L, gap width w, periodicity (center-to-center period of the structure) p_x and p_y, and angle θ variations, and in all of them $t_{Au} = 30$ nm and $t_{Ti} = 5$ nm. In Fig. 3(a), L is varied while the other parameters are kept constant. Figure 3(b) shows the w dependence of the structure. As w increases, the resonance frequency of the structure increases strongly while that at the w change is weak. In the periodicity, P, change given in Fig. 3(c), the resonance frequency of the structure is changing slightly. As can be clearly seen from Fig. 3(d), the frequency response is not affected by the angle change. Moreover, the amplitude change is negligible with θ. These observations indicate that the resonant characteristics of x-shaped nanoapertures are strongly dependent to the geometrical parameters. Therefore, one can easily tune the resonance frequency of the structure from mid-IR to visible region by changing its dimensions.

For the equivalent circuit modelling of the structure, a simple circuit design shown in Fig. 4 is used. Figure 4(a) demonstrates the numerical results (dashed line), experimental results (dot-dashed lines), and the circuit model results (solid line). To obtain a resonance around 65 THz from the x-shaped nanoantennas as shown in Fig. 4(a) the dimensions of the structure, such as L, or ω, should be changed. This simple circuit is based on the model proposed by Davis[28]. Transmission lines with the characteristic impedance of free space provide a means to propagate electromagnetic energy to and from a resonant circuit. In the proposed model, the impedance of the transmission lines is chosen to be characteristic impedance of free space to effectively simulate the wave

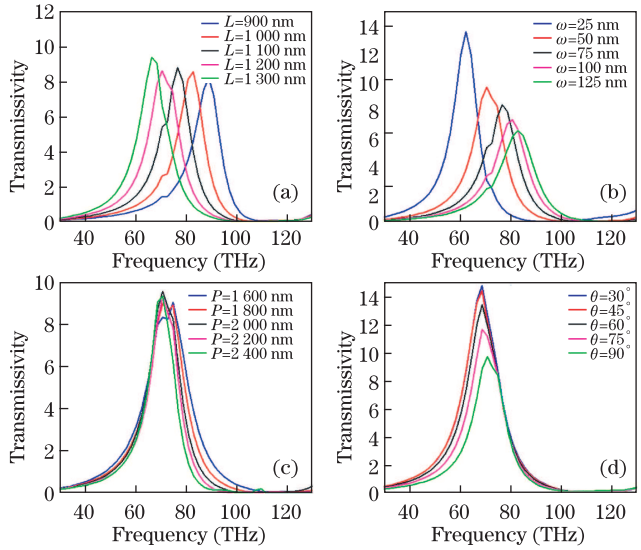

Fig. 3. Spectral response of the periodic subwavelength x-apertures. (a) L-variation at fixed $p_x = p_y = 2000$ nm, $\omega = 50$ nm, and $\theta = 90°$. (b) w-variation at fixed $L = 1200$ nm, $p_x = p_y = 2000$ nm, and $\theta = 90°$. (c) Periodicity variation at fixed $L = 1200$ nm, $\omega = 50$ nm, and $\theta = 90°$. (d) θ-variation at fixed $L = 1200$ nm, $p_x = p_y = 2000$ nm, and $\omega = 50$ nm.

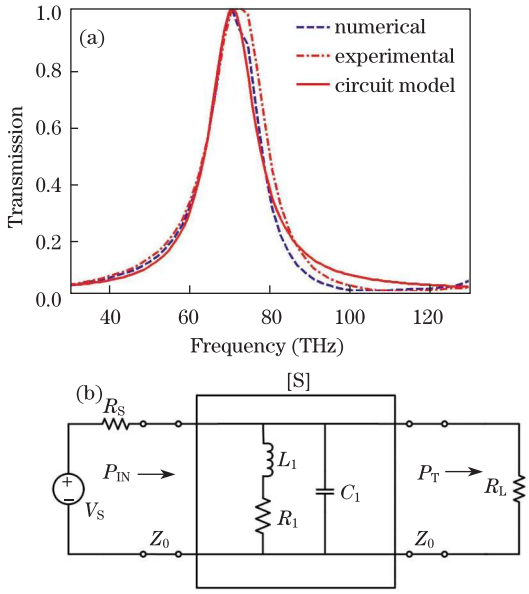

Fig. 4. (a)Transmission spectra of x-apertures for an x-polarized light source. (b) Equivalent circuit model for the resonant characteristics of the structure ($L = 1200$ nm, $p_x = p_y = 2000$ nm, $\omega = 50$ nm, and $\theta = 90°$.

propagation to and from the aperture system.

Furthermore, the load resistance, R_L, and the source resistance, R_S, are matched to the characteristic impedance of the transmission lines, Z_0, to avoid the effect of standing waves. The resonance wavelength of the aperture antenna is set by the capacitor, C_1 and the inductor, L_1 in the model circuit, as $\lambda = 2\pi/(\sqrt{L_1 C_1})$ and R_1 determines the loss in the system. The quality factor of the circuit model is then connected to the resonance wavelength and capacitance, as $Q = \pi C_1 Z_0/(\lambda)$. When the load and source resistances are matched to the characteristic impedance of the transmission line Z_0, the transmission of the system can be written as

$$\frac{P_T}{P_{IN}} = |S_{21}|^2 = 1 - \left[\frac{|(Z_{grid}||Z_0) - Z_0|}{(|Z_{grid}||Z_0) + Z_0|}\right]^2, \quad (1)$$

$$Z_{grid} = (R_1 + jwL_1)||(jwC_1)^{-1}. \quad (2)$$

Figure 4(b) demonstrates that the circuit model clearly predicts the behavior of the x-apertures. Here, we find the values of circuit elements as $C_1 = 0.075$ fF, $L_1 = 0.067$ pH and $R_1 = 1\ \Omega$ for the proposed model by matching the transmission data of the x-apertures to relevant circuit equations. We scaled the L_1 and C_1 values of the model to obtain the inductor and capacitor values. Resistor values were not scaled in this manner, instead we calculated them to give the peak power transmission equal to the simulated structure. The agreement between the results obtained from the circuit model and numerical simulations and experiments shows the efficiency of the model in predicting the resonance frequency of the x-apertures.

In conclusion, we experimentally measure and theoretically analyze the light transmission characteristics of x-shaped subwavelength apertures for operating in the mid-IR. The results are in good agreement with those obtained by numerical simulations and experiments. We theoretically analyze the physical origin of the spectral behavior by field distribution analysis. We also experimentally obtain the dependence of the spectral response on geometrical parameters. Although we study the periodic subwavelength x-aperture array operating in the mid-IR, the proposed model is not restrictive to this one and can be used to analyze different structures. It also offers an important way to understand the resonance behavior of the different metamaterials and plasmonic antennas. Using an equivalent circuit model as a designing tool, the geometry of the subwavelength structures can be optimized to achieve certain desired properties which are crucial for specific applications[29]. Such periodic subwavelength structures with tunable spectral behavior can have far-reaching consequences for chip-based frequency selective optical devices including active filters and bio- and chemical-sensors.

Profs. H. Altug, A. E. Cetin, and S. Aksu from Boston University are thanked for invaluable discussions. A two-year visiting fellowship from the Boston University for Research in Electrical and Computer Engineering and Photonics Center is gratefully acknowledged. Author also acknowledges the support from the Scientific and Technological Research Council of Turkey (TUBITAK).

References

1. T. W. Ebbesen, H. J. Lezec, H. Ghaemi, T. Thio, and P. A. Wolf, Nature **391,** 667 (1998).
2. W. L. Barnes, A. Dereux, and T. W. Ebbesen, Nature **424,** 824 (2003).
3. C. Genet and T. W. Ebbesen, Nature **445,** 39 (2007).
4. T. J. Kim, T. Thio, T. W. Ebbesen, D. E. Grupp, and H. J. Lezec, Opt. Lett. **24,** 256 (1999).

5. A. Degiron, H. J. Lezec, W. L. Barnes, and T. W. Ebbesen, Appl. Phys. Lett. **81,** 4327 (2002).
6. A. V. Itagi, D. D. Stancil, J. A. Bain, and T. E. Schlesinger, Appl. Phys. Lett. **83,** 4474 (2003).
7. E. X. Jin and X. Xu, Jpn. J. Appl. Phys. **43,** 407 (2004).
8. A. R. Zakharian, M. Mansuripur, and J. V. Moloney, Opt. Express **12,** 2631 (2004).
9. K. J. Molen, K. J. Koerkamp, S. Enoch, F. B. Segerink, N. F. Hulst, and L. Kuipers, Phys. Rev. B **72,** 045421 (2005).
10. J. H. Kim and P. J. Moyer, Opt. Express **14,** 6595 (2006).
11. E. X. Jin and X. Xu, Appl. Phys. B **84,** 3 (2006).
12. Y. J. Bao, H. M. Li, X. C. Chen, R. W. Peng, M. Wang, X. Lu, J. Shao, and N. B. Ming, Appl. Phys. Lett. **92,** 151902 (2008).
13. M. L. Brongersma, Nature Photonics **2,** 270 (2008).
14. A. A. Yanik, R. Adato, and H. Altug, J. Nanosci. Nanotechnol. **10,** 1713 (2010).
15. M. Turkmen, S. Aksu, A. E. Cetin, A. A. Yanik, and H. Altug, Opt. Express **19,** 7921 (2011).
16. J.-W. Lee, J.-K. Yang, I.-B. Sohn, H.-K. Choi, C. Kang. and C.-S. Kee, Opt. Eng. **51,** 119002 (2012).
17. E. Betzig and R. J. Chichester, Science **262,** 1422 (1993).
18. E. J. Sanchez, L. Novotny, and X. S. Xie, Phys. Rev. Lett. **82,** 4014 (1999).
19. E. Betzig, J. K. Trautman, R. Wolfe, E. M. Gyorgy, P.L. Finn, M. H. Kryder, and C. H. Chang, Appl. Phys. Lett. **61,** 142 (1992).
20. T. Kalkbrenner, U. Hakanson, A. Schadle, S. Burger, C. Henkel, and V. Sandoghdar, Phy. Rev. Lett. **95,** 200801 (2005).
21. L. Wang, S. M. Uppuluri, E. X. Jin, and X. Xu, Nano Lett. **6,** 361 (2006).
22. S. Park and J. W. Hahn, Opt. Express **17,** 20203 (2009).
23. A. Kinkhabwala, Z. Yu, S. Fan, Y. Avlasevich, K. Mullen, and W. Moerner, Nat. Photon. **3,** 654 (2009).
24. D. Austin, N. Mullin, I. Luxmoore, I. C. Sandall, A. G. Cullis, A. Bismuto, J. Faist, J. K. Hobbs, and L. R. Wilson, Appl. Phys. Lett. **96,** 151105 (2010).
25. M. Abashin, A. Agrawal, and H. Lezec, in *Proceedings of Quantum Electronics and Laser Science Conference* QTuH6 (2011).
26. Finite-difference-time-domain package, Lumerical FDTD, www.lumerical.com.
27. E. D. Palik, *Handbook of Optical Constants of Solids* (Academic, Orlando, 1985).
28. J. E. Davis, Infrared Phys. **20,** 287 (1980).
29. X. Zhang, Q. Li, W. Cao, W. Yue, J. Gu, Z. Tian, J. Han, and W. Zhang, Chin. Opt. Lett. **9,** 110012 (2011).